Available online at www.sciencedirect.com
ScienceDirect
Geochimica et Cosmochimica Acta 70 (2006) 4906–4920
Geochimica
www.elsevier.com/locate/gca

Calcification rate influence on trace element concentrations in aragonitic bivalve shells: Evidences and mechanisms

Matthieu Carré [a,*], Ilhem Bentaleb [a], Olivier Bruguier [b], Elmer Ordinola [c], Nicholas T. Barrett [d], Michel Fontugne [e]

[a] *Institut des Sciences de l'Evolution de Montpellier, Université Montpellier II, 34095 Montpellier, France*
[b] *ISTEEM, Service ICP-MS, Université Montpellier II, 34095 Montpellier, France*
[c] *Instituto del Mar del Peru, Laboratorio Costero de La Cruz, Tumbes, Peru*
[d] *DSM DRECAM SPCSI, CEA Saclay, 91191 Gif sur Yvette, France*
[e] *Laboratoire des Sciences du Climat et de l'Environnement, Domaine du CNRS, 91198 Gif sur Yvette, France*

Received 14 February 2006; accepted in revised form 17 July 2006

Abstract

Trace elements in calcareous organisms have been widely used for paleoclimatic studies. However, the factors controlling their incorporation into mollusc shells are still unclear. We studied here the Sr, Mg, Ba and Mn serial records in the shells of two aragonitic marine bivalve species: *Mesodesma donacium* and *Chione subrugosa* from the Peruvian Coast. The elemental concentrations were compared to local temperature and salinity records. The relationships with crystal growth rate *G* were investigated thanks to well defined periodic growth structures providing a precise shell chronology. Our results show that for both species, environmental parameters only have minor influence, whereas crystal growth rate strongly influences trace elements concentrations, especially for Sr (explaining up to 74% of the variance). The relationship between *G* and Sr/Ca exhibits variability among the shells as well as inside the shells. For a same growth rate value, Sr/Ca values are higher in more curved shell sections, and the growth rate influence is stronger as well. We show that intercellular and Ca^{2+}-pump pathways cannot support the calcification Ca^{2+} flux, leading us to propose an alternative mechanism for ionic transport through the calcifying mantle, implying a major role for calcium channels on mantle epithelial cell membranes. In this new calcification model, Sr/Ca shell ratios is determined by Ca^{2+}-channel selectivity against Sr^{2+}, which depends (i) on the electrochemical potential imposed by the crystallisation process and (ii) on the Ca^{2+}-channel density per surface unit on mantle epithelia.

1. Introduction

Trace elements in calcareous organisms have been widely used for paleoclimatic studies. However, their incorporation into biogenic carbonates is only partially controlled by environmental factors. A calcareous skeleton is the result of a mineralization process, biologically controlled and genetically programmed (Wheeler, 1992). The genetic influence on Sr and Mg incorporation is evidenced by the important concentration differences existing between taxonomic groups (Chave, 1954; Dodd, 1967). In some groups, the biological effect (often called "vital effect") is constant enough to allow paleoenvironmental studies provided that a specific relationship is calibrated, like for sclerosponges (Rosenheim et al., 2005) or corals (Beck et al., 1992; Gagan et al., 2000; Marshall and McCulloch, 2002; Cobb et al., 2003; Corrège et al., 2004; Yu et al., 2005). On the other hand, the studies aiming to use trace elements in mollusc shells as environmental proxies give disparate results. For the widely studied species *Mytilus edulis*, Dodd (1965) first suggested that sea surface temperature (SST) was recorded by Sr/Ca ratios, which was later shown to be highly uncertain (Klein et al., 1996a; Vander Putten et al., 2000). The temperature dependence of Mg/Ca ratios was also reported

* Corresponding author. Fax: +33 4 67 14 36 10.
E-mail address: carre@isem.univ-montp2.fr (M. Carré).

0016-7037/$ - see front matter © 2006 Elsevier Inc. All rights reserved.
doi:10.1016/j.gca.2006.07.019

in two mollusc species (Klein et al., 1996b; Takesue and van Geen, 2004). However, the environmental control on minor and trace elements in molluscs seems often too weak to develop suitable proxies. Actually, the mechanisms controlling the trace element incorporation in mollusc shells remain largely unknown. For Klein et al. (1996a), Sr incorporation is modulated by metabolic efficiency in the mantle epithelium. Nevertheless, there is growing evidence that calcification rate (or crystal growth rate) exerts a strong positive influence on the shell Sr concentration (Gillikin et al., 2005; Stecher et al., 1996; Takesue and van Geen, 2004), even though this was not demonstrated until now.

We studied here the Sr, Mg, Ba and Mn serial records in the shells of two aragonitic marine bivalve species: *Mesodesma donacium* and *Chione subrugosa* from the Peruvian Coast. Our aims are (1) to investigate the mechanisms controlling the metallic ions incorporation into the shell aragonite and (2) to identify potential paleoenvironmental indicators. A particular attention was devoted to the shell crystal growth rate effects. Thanks to well-defined sclerochronologies (chronology based on shell growth lines) (Carré, 2005; Carré et al., 2005), high-resolution geochemical studies as well as precise calcification rate evaluations are possible using these species.

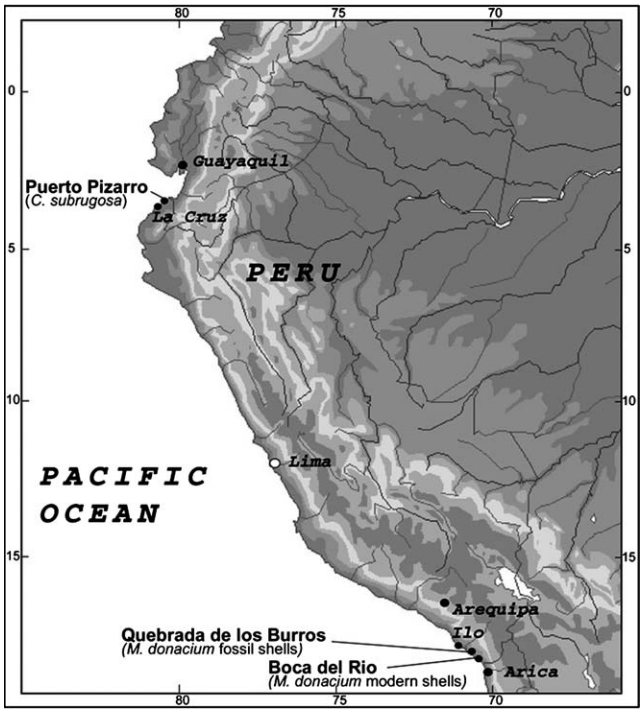

Fig. 1. Geographic locations of the shell collection sites.

2. Material and sites

2.1. Mesodesma donacium

Mesodesma donacium is a surf clam living on the high energy sandy beaches of Chile and Peru, at depths from 0 to 10 m. Four shells were analysed. Three of them were collected alive in 2003 at ~1 m depth during the low tide on the beach of Boca del Rio (18.1°S) in the southernmost Peru (Fig. 1). The last one comes from the nearby archaeological site "La Quebrada de los Burros" (Fig. 1) and is dated at about 9200 Cal. Yr BP (Table 1) (Fontugne et al., 1999; Lavallée et al., 1999). There is no freshwater runoff in this extremely arid area (precipitation is less than 10 mm/yr). The mean SST is about 16 °C and the salinity is stable (~35).

2.2. Chione subrugosa

This bivalve lives in the intertidal zone of mangrove lagoons from northern Peru to Mexico. The exceptional definition of the growth lines in the shells provides an excellent chronology for geochemical records (Carré, 2005). We analysed two shells, collected alive in the lagoon of Puerto Pizarro in northern Peru in 2002 and 2004 (Fig. 1, Table 1). In this region, precipitations are concentrated between February and May and can be extremely strong during El Niño events. The mean SST is about 27 °C. Salinity is ~34 and usually drops to 29 in the rainy season. As the lagoon is not directly connected to the river delta and is drained and filled twice a day by the tides, the conditions are close to those of the open sea.

2.3. Environmental data

Coastal SSTs in Boca del Rio, southern Peru (18.1°S), were interpolated using two daily SST records measured in Ilo, Peru (Instituto del Mar del Peru (IMARPE) coastal station), and from Africa, Chile (Centro Nacional de Datos Oceanográficos de Chile (CENDOC), Servicio Hidrográfico y Oceanográfico de la Armada de Chile (SHOA)). The validity of such interpolation has been verified from July to December 2003 (for more details, see Carré et al., 2005). Salinity time series are not available for this locality. In Puerto Pizarro, northern Peru (3.4°S), monthly SSTs were provided by the FONDEPES (Fondo Nacional de Desarollo Pesquero). Salinity time series of the open sea were measured and supplied by the IMARPE coastal station en La Cruz (3.5°S).

3. Methods

3.1. Shell preparation

The live-collected shells were immediately sacrificed and their flesh removed. Shells were cleaned, embedded directly in polyester resin without any chemical treatment, and radially sectioned using a diamond wire saw with 0.3 mm diameter wire. All sections (~1 mm thick) were polished, rinsed with demineralised water then with ethanol, air-dried, and finally photographed under reflected light through a binocular microscope. As shown in Fig. 2, the shell brmd19 was sectioned along a short growth axis (Sx), the shell N6-2 along the long growth axis (Lx) and the shells brmd21 and brmd24 along both axes. The shells PPCS1 and CM26-3 were sectioned along central radial axis (Fig. 3).

Along the long growth axis of brmd24 and brmd21, two parallel sections were extracted for trace elements and stable isotope analyses.

3.2. Minor and trace elements analyses

Shell sections were cut in ~1 cm long pieces and embedded in polyester resin cylinders. The analysed surface was polished and cleaned with ethanol. High resolution Sr/Ca, Ba/Ca, Mg/Ca, and Mn/Ca ratios measurements were carried out at ISTEEM on a

Table 1
Geographic origin, code, length, and collection date of the shells studied

Species	Shell code	Length (mm)	Collection site	Coordinates	Collection date, age of fossil
Mesodesma donacium	brmd19	68	Boca del Rio	18°10′ S 70°39′ W	27/01/2003
	brmd21	66			31/03/2003
	brmd24	75			18/06/2003
	N6-2	57	Quebrada de los Burros	18°01′ S 70°50′ W	9000 à 9400 cal. BP
Chione subrugosa	PPCS1	46	Puerto Pizarro	3°31′ S 80°24′ W	24/07/2002
	CM26-3	36			26/03/2004

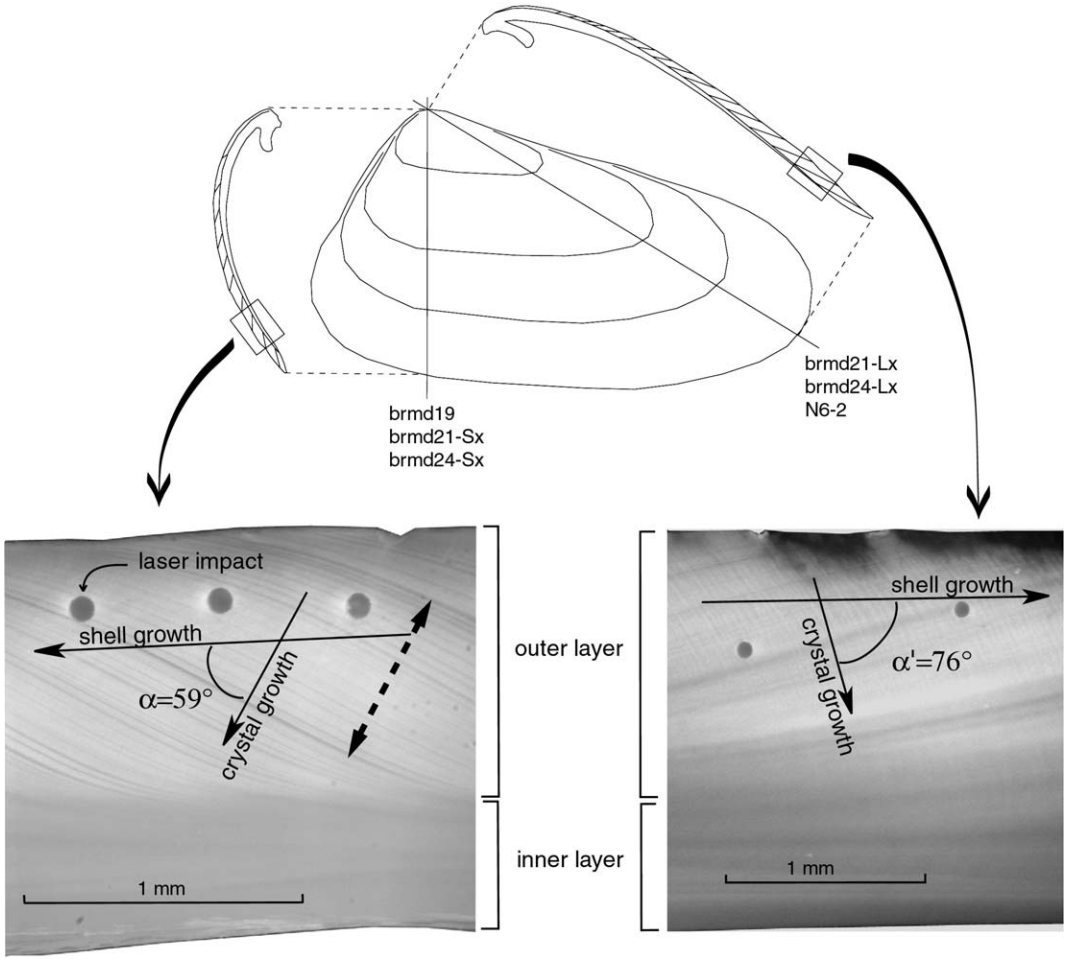

Fig. 2. Schematic representation of a *M. donacium* valve and of the two radial axis along which shells were studied. Profile codes are indicated in front of the corresponding axis. Shell sections are also represented. Photographs show details of analysed shell sections for each axis. Growth lines are apparent and underlined by the black lines. The thin arrows indicate the shell growth direction, forming the angle α with shell growth direction. The dashed arrow represents a fortnightly growth cycle and also shows the crystal growth direction. Laser impacts are visible as dark discs (Ø 77 μm).

laser-ablation inductively coupled plasma mass spectrometer (LA-ICPMS) using a deep UV laser source. The system characteristics are reported in Table 2. We used ^{43}Ca as internal standard, and NIST 610 and NIST 612 as external standards, as described by Vander Putten et al. (1999), using the concentrations reported by Pearce et al. (1997). The analytical precision is better than 5% for Sr/Ca and 10% for the other elements. The laser impacts have a 77 μm diameter and are spaced by 0.25–1 mm along the growth direction, depending on the shell growth rate. For each species, 7 short analyses series (2–4 spots) were made following a single growth line. After the analyses, shell sections were photographed for sclerochronological analyses (see Section 3.4).

3.3. $\delta^{18}O$ analyses

Two shell sections, brmd21-Lx and brmd24-Lx (Lx = long axis, Sx = short axis), were sampled at high resolution with an automatized microdrilling device

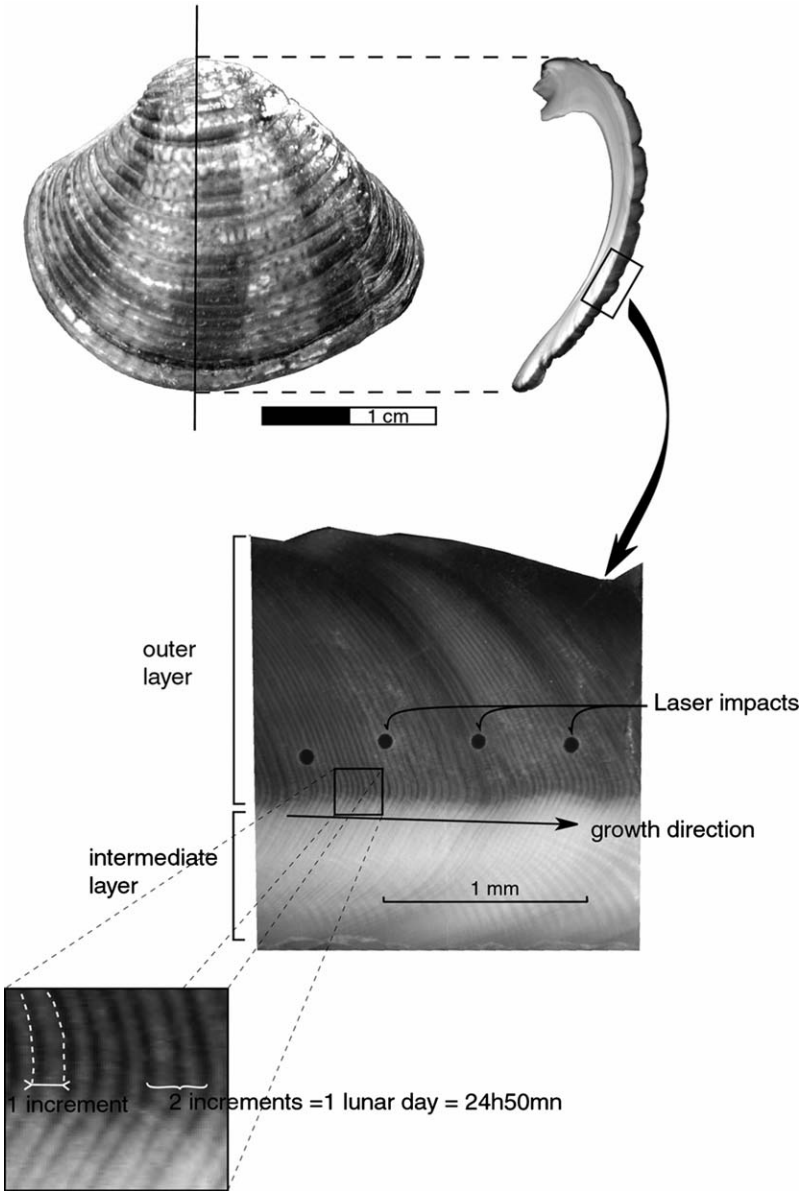

Fig. 3. Photograph of a *C. subrugosa* valve, the cutting axis and the corresponding section view. The photograph in the middle shows a section detail. The outer layer and the intermediate layer are clearly separated. The inner layer is not shown. Laser impacts are indicated (Ø 77 μm). Growth lines are also clearly visible. The microincrement limits are indicated on the enlarged view below. Two microincrements represent one lunar day.

(Merchantek MICROMILL™). Sample grooves are ~0.2 mm large and 0.2 mm deep, and follow the inner growth line direction. Powdered calcium carbonate samples weight between 50 and 100 μg. The isotopic ratios were determined using an automated carbo-device coupled with a Dual Inlet Optima-VG mass spectrometer. Carbonate samples were acidified with 100% phosphoric acid liberating the CO_2 for subsequent analysis on the mass spectrometers. The results are calibrated versus the NBS-19 international standard and given in the conventional δ-notation expressed in permil against the V-PDB standard (Vienna Pee Dee Belemnite) where:

$$\delta O^{18}(\text{Sample}) = (R_{\text{sample}}/R_{\text{reference}} - 1) \times 10^3 \qquad R \text{ is } {}^{18}O/{}^{16}O.$$

Reproducibility is 0.05‰.

3.4. Shell chronology

A precise chronology was reconstructed for the elemental and isotopic profiles using the periodicities of the inner shell growth lines. Each sample in a shell section can be dated by counting the periodic structures separating it from the shell margin which corresponds to the date of death. As many subtidal and intertidal bivalves, the inner shell growth lines in *M. donacium* and *C. subrugosa* are formed during the low tides (Evans, 1975; Rhoads and Lutz, 1980; Carré, 2005; Carré et al., 2005). For *M. donacium*, daily tidal lines are not always identifiable but form fortnightly clusters in response to the succession of spring and neap

Table 2
LA-ICP-MS system characteristics

ICP-MS	
Model	VG PQ2 turbo ("option S")
Forward power	1350 W
Reflected power	<5 W
Cool gas	14 L/min
Auxilliary gas	0.8 L/min
Carrier gas	0.9 L/min
Laser	
Laser type	Compex 102
Wavelength	193 nm
Laser mode	Q-Switched
Repetition rate	5 Hz
Primary output power	160 mJ
Pulse width	15 ns
Ablation medium	He
	1.2 L/min
Spot size	77 μm
Acquisition parameters	
Detector mode	PC
Dwell time/isotope	Variable
Quad settle time	10.24 ms
Points/peak	3
Pre-ablation time	10 s
Acquisition time	20 s
No. of repeats	3

tides. We used the fortnightly lines (their mean period is 14.8 days) to reconstruct a time axis in *M. donacium* shells (more details are given in Carré et al. (2005)). Semi-lunar day periodic (12h25mn) lines were used for *C. subrugosa* since they are exceptionally well defined (Carré, 2005), as can be seen in Fig. 3.

3.5. Growth rate calculation

For practical reasons, the shell growth rate is often studied as the linear shell extension rate G_L (Gillikin et al., 2005; Klein et al., 1996a). However, it is physically more relevant to consider the crystal growth rate G (μm/day) (Carpenter and Lohmann, 1992). Assuming a constant density of the aragonite in the outer shell layer, G is proportional to the calcification rate per surface unit R (g/mm^2/day). It is measured along the direction perpendicular to the mineralization front which is materialized by the growth lines. The shell extension rate depends on G and α, the angle between the shell growth direction and the crystal growth direction (Fig. 2): $G_L = G/\cos(\alpha)$. Because α varies with the growth direction and with ontogeny (Fig. 2), G_L is not a suitable parameter to study the growth influence on shell geochemistry.

In all shells, we estimated G for each laser spot using the periodic growth structures:

$G = d/T$, where T is the period and d the distance between two consecutive periodic lines. d was measured perpendicularly to the growth lines, with the picture analysis software Optimas®. In *C. subrugosa* shells, laser spots are generally overlapping several micro-increments (Fig. 3). In this case, the mean value for all impacted increments is attributed. The error on G values depends on the errors on d and T. For *C. subrugosa*, T is clearly fixed at 12h25mn (1 microincrement). However, the T value (14.8 days) for *M. donacium* shells implies an error of ~3 days (~20%) because spring tides are not exactly periodic (Carré, 2005). The uncertainty on d values is ~1% for *M. donacium* and ~10% for *C. subrugosa*. Finally, the uncertainty on G estimations is about 21% for *M. donacium*, and 10% for *C. subrugosa*.

4. Results

In Figs. 4 and 5, minor and trace elements profiles and growth rate values are represented for all shells against a time axis, as well as isotopic and environmental data when available. All values are available in electronic annex 1.

4.1. Growth rate

For *M. donacium*, the growth rate varies generally between 10 and 50 μm/day but it can reach 80 μm/day in the shell brmd21. *Chione subrugosa* growth rates are comprised mainly between 10 and 120 μm/day. A decreasing trend during ontogeny is observed for both species. This trend is not visible in the fossil shell N6-2 because the juvenile part, where the main growth rate variation occurs, was not studied owing to its bad preservation.

For the twice-cut shells brmd21 and brmd24, growth rate curves of both axes are superposed on the same graph (Fig. 4). In both shells, the growth rate values are similar along both directions, despite the important difference of linear shell extension rate (Fig. 2). This result indicates that, for this species, the calcification rate is constant along the mineralizing edge of the shell and that the section length differences are only due to the differences between α and α' angles (Fig. 2).

No significant correlation between growth rate and SSTs is evidenced in these curves.

4.2. Minor and trace elements

For all elements, the concentrations follow a general, more or less pronounced, decreasing trend as a function of time, although elemental profiles are flatter in N6-2 shell. Mn/Ca ratios for CM26-3 and Mg/Ca ratios for brmd19, brmd21-Sx, and brmd24-Sx are not shown because the Mn and Mg concentrations were below the ICP-MS detection limit.

The mean Sr/Ca ratios are comprised between 2.2 and 2.8 mmol/mol for *M. donacium* and are 2.2 and 3.6 mmol/mol for *C. subrugosa*. In shell brmd21 juvenile phase, Sr/Ca values are slightly higher on the short axis than on the long one, and are similar later. In shell brmd24, the Sr/Ca difference between the long and short axis is larger (from 1 to 1.5 mmol/mol) during the whole shell life.

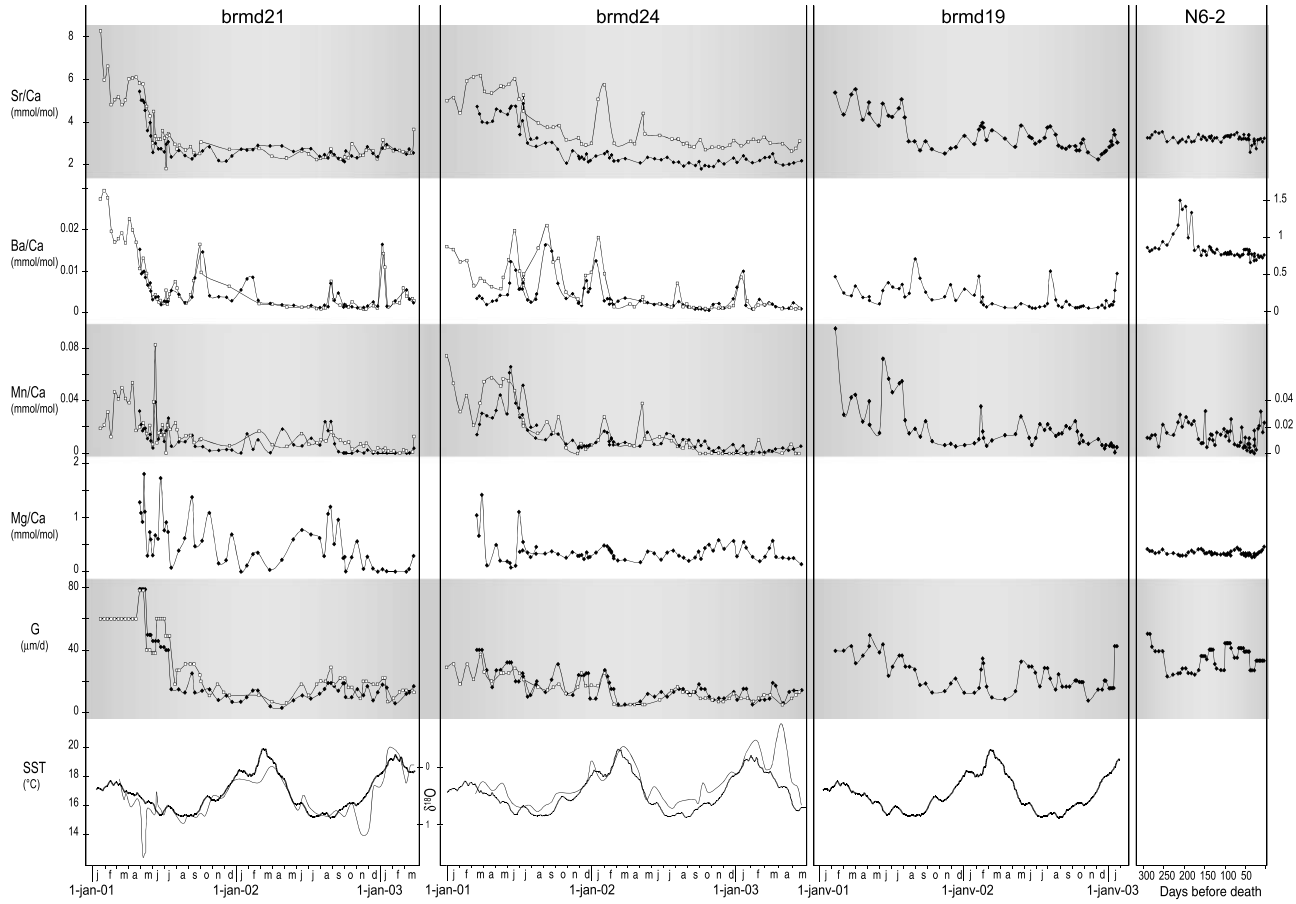

Fig. 4. Sr/Ca, Ba/Ca, Mn/Ca, and Mg/Ca values of the *M. donacium* shells expressed in mmol/mol. The profiles are positioned on a time axis reconstructed from growth line analysis (for more details, see Carré et al., 2005). Mg/Ca values are not shown for brmd19 because they were inferior to the system detection limit. Crystal growth rate G is expressed in µm/day. Weekly SSTs (bold line) and $\delta^{18}O$ (thin line), expressed in ‰ vs. VPDB, are represented below. For brmd21 and brmd24, values of the short sections (□) and of the long sections (◆) are shown together.

Ba/Ca ratios are low in all contemporary shells, with mean values below 0.02 mmol/mol. The mean value in the fossil shell N6-2 is 0.085 mmol/mol. This higher value might indicate environmental changes. The Ba concentrations along the two axes are similar in brmd21 whereas in brmd24, they are higher in the short axis compared to the long axis.

Mn/Ca mean values range from 0.001 mmol/mol in N6-2 to 0.014 mmol/mol in brmd24-Sx. For both species, the juvenile parts contain the highest values weakening later. The shell brmd24 is initially enriched along the short axis compared to the long axis.

Mg/Ca mean values range from 0.29 mmol/mol (N6-2) to 0.59 mmol/mol (brmd21-Lx). The profiles decrease slightly. It is worth noting that Mg concentrations were below the detection limit on brmd21 and brmd24 short axis but not on the long axis. Therefore, the long axes are enriched in this case, contrary to what is observed for the other elements.

Analyses along a unique growth line provide information about the elemental profile reproducibility (see electronic annex 2). In *M. donacium* shells, Sr/Ca deviation along a single growth line is less than 6%, except in one series which attains 14.6% deviation. For *C. subrugosa*, relative Sr/Ca deviations are comprised between 5% and 28%. These larger inner variations can be attributed to microstructural changes since the replicates were measured in the intermediate shell layer for this species (Fig. 3). No systematic trend is observed along growth lines.

4.3. Correlations with temperature (SST), salinity (SSS), and crystal growth rate (G)

All linear correlation coefficients (r), with the values number N, are reported in Table 3. For *C. subrugosa*, only the measurements in the outer layer were included in the correlation calculations. There is no significant correlation with temperature or salinity, except in two cases: (Sr/Ca–SST) in CNM26-3 and (Mg/Ca–SST) in brmd21-Lx. In all shells, the strongest correlation occurs for the couple (Sr/Ca–G). For these variables, r values range from 0.49 in N6-2 to 0.86 in brmd21-Lx. The correlation is weaker for N6-2 because we only analysed the adult period, when G is more stable. r(Sr/Ca–G) is better than 0.7 for 5 out of 8 profiles. Except for N6-2, significant correlations are also observed between G and Mn/Ca, with a r maximum of

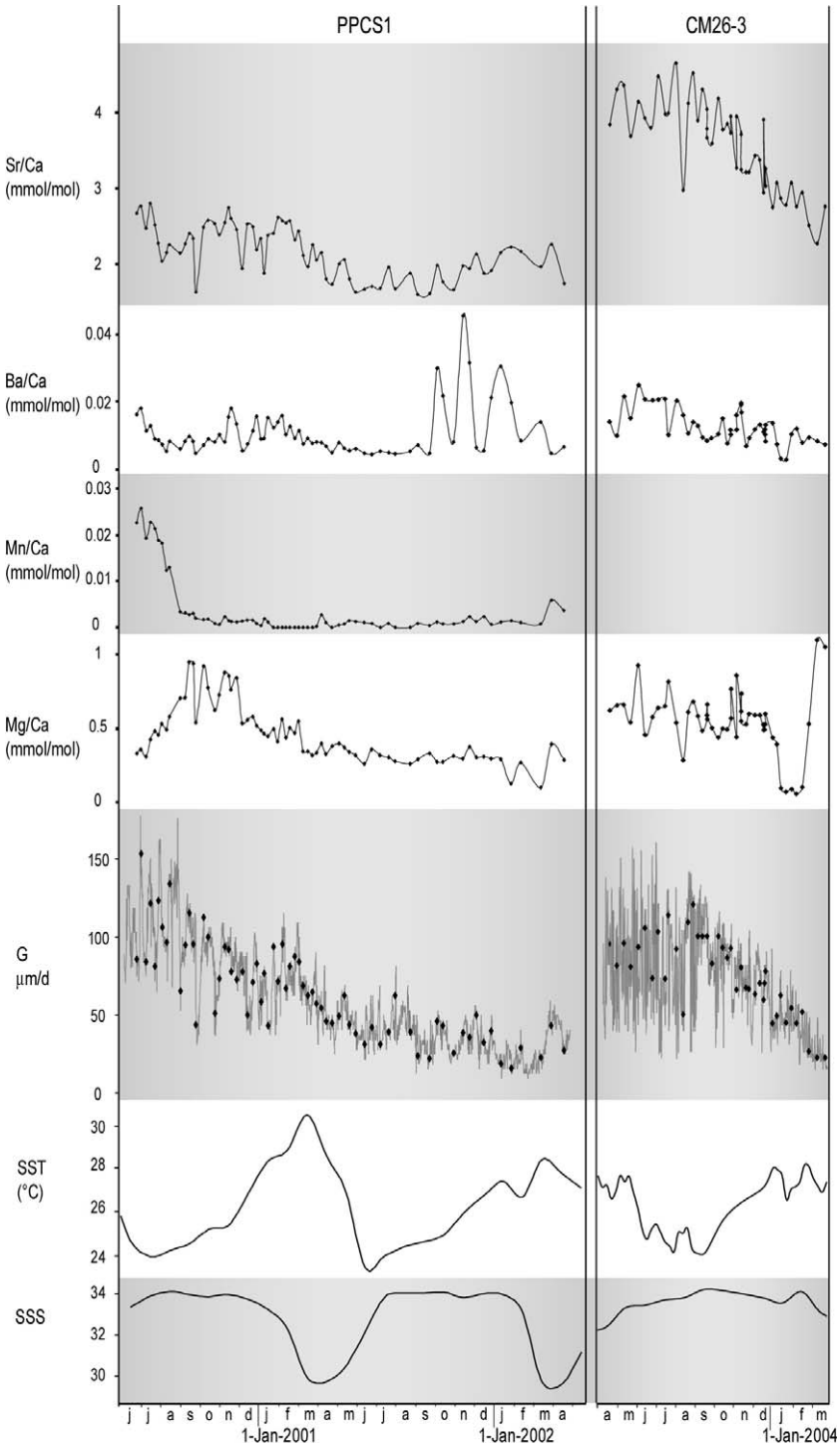

Fig. 5. Sr/Ca, Ba/Ca, Mn/Ca, and Mg/Ca values of the *C. subrugosa* shells expressed in mmol/mol. Crystal growth rate *G* is represented at the microincrement level, black diamonds represent the values corresponding to the laser impacts. Monthly values of SST and open sea salinity are shown below.

0.74 in brmd24-Sx. All the significant correlations related to *G* are positive. The only two significant correlations related to SSTs are negative.

The linear regressions between Sr/Ca (mmol/mol) and *G* (μm/day) are reported in Fig. 6. The slopes d(Sr/Ca)/d*G* are comprised between 0.012 and 0.117 for *M. donacium* and between 0.007 and 0.021 for *C. subrugosa*. Thus, the discrepancy among slope values reaches one order of magnitude. The variability of Sr/Ca dependence on growth rate is observed among the species, individuals and even within shells. As a matter of fact, the slope values of the Sr/Ca–*G* relationships in long and short sections are statistically different (99% confidence level) in both twice-cut shells (for the statistical method, see Neuilly and Cetama, 1998, pp.

Table 3
Correlation coefficients r between elemental concentrations (mmol/mol) and the variables SST (°C), SSS (salinity) and G (mm/day)

	Variables / Shells	Sr/Ca			Ba/Ca			Mn/Ca			Mg/Ca		
		SST	SSS	G	SST	SSS	G	SST	SSS	G	SST	SSS	G
Mesodesma donacium	brmd19	-0.048 (61)	-	0.718 (61)	-0.072 (61)	-	0.311 (61)	-0.261 (61)	-	0.529 (61)	-	-	-
	brmd21 Lx	0.041 (55)	-	0.859 (55)	0.093 (55)	-	0.472 (55)	-0.331 (42)	-	0.617 (42)	-0.531 (49)	-	0.611 (49)
	brmd21 Sx	0.099 (64)	-	0.767 (64)	0.149 (64)	-	0.601 (64)	-0.159 (63)	-	0.557 (63)	-	-	-
	brmd24 Lx	-0.291 (73)	-	0.697 (73)	-0.112 (73)	-	0.242 (73)	-0.376 (73)	-	0.584 (73)	0.027 (72)	-	0.364 (72)
	brmd24 Sx	-0.079 (58)	-	0.822 (58)	-0.151 (58)	-	0.664 (58)	-0.066 (46)	-	0.737 (46)	-	-	-
	N6-2	-	-	0.486 (55)	-	-	-0.351 (55)	-	-	-0.216 (55)	-	-	0.220 (55)
Chione subrugosa	PPCS1	-0.089 (69)	0.179 (65)	0.666 (69)	0.116 (69)	0.224 (65)	-0.066 (69)	-0.359 (57)	0.195 (53)	0.635 (57)	-0.272 (69)	0.284 (65)	0.610 (69)
	CM26-3	-0.531 (50)	0.074 (43)	0.852 (50)	-0.144 (50)	-0.151 (43)	0.326 (50)	-	-	-	-0.300 (50)	-0.348 (43)	0.187 (50)

The number of value couples N is indicated in the right bottom corner of each division. Divisions are coloured in grey when the correlation is significant ($p < 0.001$), and in dark grey when the correlation is strong ($r > 0.7$).

367–369). Sr/Ca dependence on crystal growth rate is stronger along the short axis than the long one. The lowest slope is found in N6-2 which was analysed on a long axis.

Correlations between element concentrations are sometimes very strong. r(Sr/Ca–Ba/Ca) reaches 0.84 in brmd21-Sx and r(Sr/Ca–Mn/Ca) reaches 0.87 in brmd24-Lx.

5. Discussion

5.1. Controlling factors

From the correlation coefficients reported in Table 3, temperature and salinity have only a minor influence on trace element incorporation into shell aragonite for the species studied here. The correlations with SST or SSS are not more significant if considering only the adult period (result not shown), showing that environmental variables influence is still weak when growth is constant. Nor do shell Sr/Ca and Mg/Ca variations reflect sea water Sr/Ca and Mg/Ca changes, since these ratios are highly stable for salinities down to 10‰ (Dodd and Crisp, 1982), which is never reached in the present study.

Positive correlations have been observed in some mollusc species between temperature and Sr/Ca or Mg/Ca ratios (Dodd, 1965; Stecher et al., 1996; Klein et al., 1996b, Vander Putten et al., 2000; Gillikin et al., 2005). However, Sr/Ca ratios in inorganic aragonite are inversely correlated to water temperature (Kinsman and Holland, 1969). Therefore, the positive Sr/Ca–SST correlations cannot be induced by thermodynamics of carbonate precipitation but rather by an indirect SST positive effect on growth rate (Stecher et al., 1996; Gillikin et al., 2005). Our results on the aragonitic species *M. donacium* and *C. subrugosa* support the increasing evidence that water temperature and salinity have a minor influence on Sr, Mg, Ba and Mn concentrations in mollusc shells.

Ba and Mn have been reported to be potential primary productivity proxies (Lazareth et al., 2003), however, our Ba and Mn profiles do not exhibit periodicity that could be related to the periodic planktonic blooms.

5.1.1. Calcification rate influence

The growth rate influence on trace element incorporation in mollusc shells has been often suggested, though without quantitative crystal growth rate studies (Pilkey and Goodell, 1963; Dodd, 1965; Stecher et al., 1996; Takesue and van Geen, 2004). The issue is still not clear since no relationship was shown in *M. edulis* calcite between Sr/Ca ratios and growth rate (Klein et al., 1996a; Lorens and Bender, 1980). Gillikin et al. (2005) studied Sr/Ca ratios and annual growth rates in two aragonitic marine bivalves, *Saxidomus giganteus* and *Mercenaria mercenaria*. A strong correlation appeared for the first species but not for the second. Gillikin et al. (2005) also aimed to study the growth rate influence at a more precise scale, reconstructing a time scale by comparing $\delta^{18}O$ profiles and temperature records as described in Klein et al. (1996a). We argue that these methods are not reliable for our purpose because (1) growth rate estimations are highly imprecise and (2) the growth rate considered is a linear shell extension rate which has no physical meaning as shown in Sections 3.5 and 4.1.

The parameter G studied here is the crystal growth rate, which is proportional to the calcification rate per

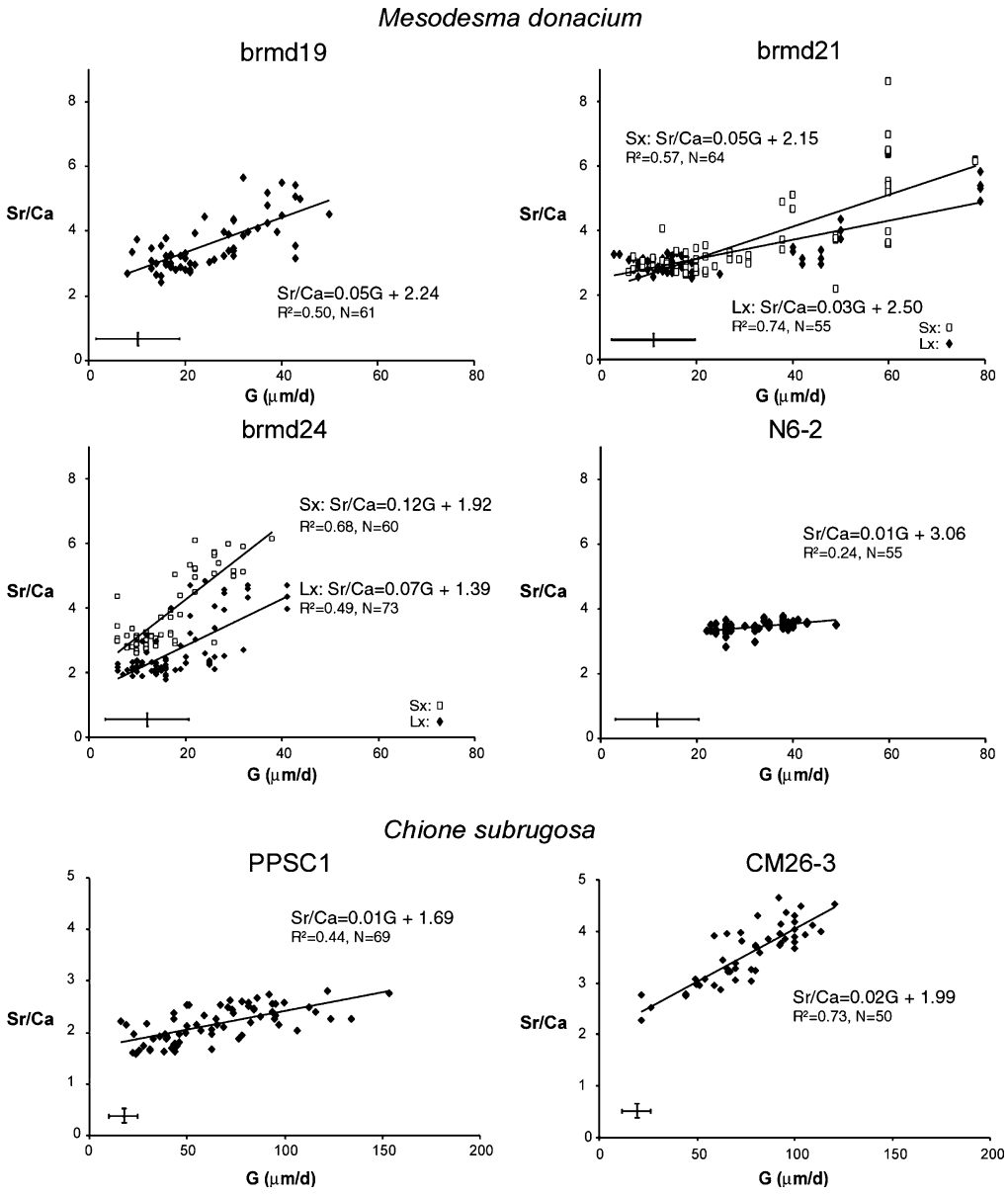

Fig. 6. Linear regressions between Sr/Ca (mmol/mol) values and the crystal growth rate G (μm/day) for each shell section. The equation, correlation coefficient R^2 and number of values N are indicated for each regression. For brmd21 and brmd24, short and long sections are distinguished as in Fig. 4. The standard error on Sr/Ca ratios and G are represented by the crosses.

surface unit, assuming a constant shell aragonite density. Our geochemical profiles, sustained by precise sclerochronological models, show the role of G in determining Sr/Ca ratios at a daily scale for *C. subrugosa*, and intramonthly scale for *M. donacium*. A relationship also exists, to a lesser extent, with Mn incorporation. Ba/Ca ratios exhibit rapid variations with large relative amplitude, especially in the early life periods. In *M. donacium* shells, G appears to be slightly better correlated to logarithmic Ba/Ca values (r up to 0.73 for brmd24-Sx), suggesting a non-linear relationship. Ba^{2+} concentration in sea water is very low (~34 nmol/L) so that Ba incorporation is expected to be highly dependent on its availability. Ba is thought to be filtered and ingested in a particulate state associated to planktonic organic matter (Lazareth et al., 2003), so that its incorporation should be also related to primary productivity and to metabolic activity. The crystal growth rate influence shown is only partial since it explains up to 74% of Sr/Ca variations in the shells studied here (54% for Mn and 44% for Ba). Even if SST certainly has a partial influence, no significant SST signal could be extracted by correcting the Sr/Ca values from calcification rate effect, because the relative error on corrected Sr/Ca values becomes to high.

5.2. The mechanisms controlling Sr^{2+} incorporation into aragonitic shells

In the rest of the article, the discussion is focused on Sr/Ca ratios and aims to identify the mechanisms through which crystal growth rate influences shell Sr/Ca ratios. As shown in previous section, environmental factors such as temperature and salinity have negligible impact. On the other hand, Sr^{2+} incorporation in inorganic aragonite is independent of the precipitation rate (Zhong and Mucci, 1989). Therefore, the Sr^{2+} discrimination mechanism has to be principally biological. Sr^{2+} discrimination can occur at two levels: (1) during shell crystallization as suggested by Gillikin et al. (2005) or (2) during the transport from the surrounding medium to the extrapallial fluid (EPF) (Fig. 7) as suggested by Klein et al. (1996a).

5.2.1. Is Sr^{2+} discriminated during mineralization?

The shell crystalline phase is tightly bound to the organic matrix, which has been shown to control the calcification timing (Wheler et al., 1981; Wheeler, 1992), calcium carbonate polymorph (Belcher et al., 1996; Falini et al., 1996) and microstructure (Addadi et al., 1992). The organic phase (matrix and enzymes) could also have an influence on the shell chemical composition. Shell organic matrix controls the crystal formation through complex mechanisms involving calcium binding sites (Wheeler, 1992; Addadi et al., 1992). If we assume that the organic phase is responsible for Sr^{2+} discrimination, this has to be the consequence of higher chemical affinities for Ca^{2+} than for Sr^{2+} at the binding sites, either on enzymes or on matrix. In such conditions, the discrimination against Sr^{2+} would depend on the binding site saturation rate: the more saturated, the less efficient is the selectivity on binding sites. Thus, growth rate would influence Sr^{2+} discrimination by its indirect relationship with binding site saturation rate. Variations of organic matrix concentration in biominerals could account for the variability of the *G*–Sr/Ca relationship among species, shells, as well as inside shells. Rosenberg and Hughes (1991) showed by measuring mantle metabolic activity and *S* concentrations in bivalve and brachiopod shells, that the outer layer contains more organic matrix in curve (short) sections than in flat (long) sections.

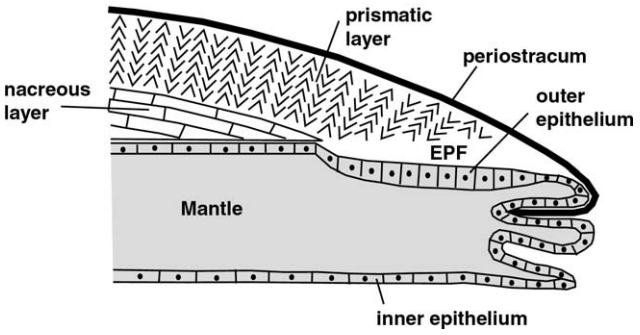

Fig. 7. Schematic bivalve radial section showing the shell edge and the mantle. EPF is the extrapallial fluid.

Therefore, binding sites should be less saturated in short sections, so that Sr/Ca ratios would be lower as well as *G* influence. This is the opposite of what we measured in shells. As a consequence, organic matrix is not responsible for crystal growth rate effect observed here. Therefore, Sr^{2+} discrimination occurs upstream, during the ionic transport to the EPF. Additional evidence supporting our conclusion is provided by Wada and Fujinuki (1976) who measured that Sr/Ca ratios in marine bivalve EPF is ~30% higher during growth periods than during rest periods (except for *Crassostreas gigas*). This shows that growth effect on Sr^{2+} incorporation occurs before the mineralization process.

5.2.2. Crossing the membranes

Only two pathways are generally considered for Ca^{2+} transport through calcifying mantle (Wheeler, 1992; Klein et al., 1996a; Gillikin et al., 2005): (1) a passive non-selective intercellular pathway and (2) an active (energy consuming) selective intracellular pathway involving Ca^{2+}-ATPase enzymes (Ca^{2+}-pump). Klein et al. (1996a) suggested that shell Sr/Ca depends on the relative importance of these two ionic pathways in the total Ca^{2+} efflux through the membranes.

We will show here that none of these two pathways can bear the Ca^{2+} flux necessary for biomineralization. A relatively low crystal growth rate corresponds to an important Ca^{2+} flux *J* through the membrane: considering an aragonite density value of 2.93 and for a growth rate $G = 20$ μm/day, $J = 4.1 \times 10^6$ ions/s/μm^2 (588 nmol/day/mm^2). A non-selective intercellular diffusion cannot be responsible for such a large flux because the membrane would no longer exert its role of chemical isolation between the physiological and the surrounding environments (in a medium *M. donacium* specimen, the physiological fluid salinity would vary by 10 psu/h in response to environmental changes). This pathway, used by all kind of ions, allows necessarily a limited flux because the hemolymphatic fluid has a chemical composition different from sea water or EPF (Wilbur and Saleuddin, 1983). Experiments using radiocalcium ^{45}Ca showed that the Ca^{2+} route is principally intracellular (Istin and Maetz, 1964; Istin and Masoni, 1973). However, the intracellular pathway involving Ca^{2+}-ATPase is unable to support such a flux since a single enzyme typically transports ~100–200 ions/s (McWhirter et al., 1987; A.G. Lee, personal comm.). Thus, in order to generate the necessary Ca^{2+} flux, cellular membranes should be entirely constituted of Ca^{2+}-ATPase [Ca^{2+}-ATPase surface is about 17 nm^2 (Taylor et al., 1986)], which is not realistic. As a consequence, an alternative intracellular pathway through membranes must exist, allowing high rate Ca^{2+} transport as well as ionic selection.

5.3. A new calcification model: the role of ionic channels

We propose here a new model for Ca^{2+} transport through mollusc mantle, involving calcium channels, which

are widespread in all kind of biological tissues (for a review, see Hagiwara and Byerly, 1981). A calcium channel is a protein forming an aqueous pore in the membrane bilayer, facilitating Ca^{2+} diffusion thanks to a succession of suitable binding sites. Ions are selected at the entrance by the pore diameter and chemical affinities on binding sites (Hess and Tsien, 1984; Dang and McCleskey, 1998; Gillespie and Eisenberg, 2002; Sather and McCleskey, 2003). Such pores are selective, diffusive (no energy is consumed), and can support very high ionic fluxes ($\sim 10^6$ Ca^{2+}/s) (Sather and McCleskey, 2003). Therefore, calcium channels are suitable candidates for Ca^{2+} transport from the surrounding medium to the EPF. Our hypothesis is supported by experiments showing that the mollusc mantle permeability is 10-fold higher for Ca^{2+} than for other ions (Coimbra et al., 1988). A bioelectric potential across the mantle membranes is generated by local Ca^{2+} concentration gradients (Istin and Kirschner, 1968).

Thus, diffusion is activated by a Ca^{2+} concentration gradient across the membrane maintained by the biomineralization process. The calcium carbonate precipitation is activated by the organic matrix and enzymatic activity in the EPF (Marin and Luquet, 2004; Milet et al., 2004), and acts as a pump for Ca^{2+} transport from the surrounding medium. Four membranes have to be crossed from sea water to EPF. Wada and Fujinuki (1976) EPF analyses for marine bivalves show that EPF cations concentrations decrease during growth creating an electrochemical potential with sea water. Although few is known about Ca^{2+} concentrations in the mantle tissue, Istin and Masoni (1973) showed that calcium circulates in interstitial hemolymphatic spaces between the inner and outer epithelia. It may be sometimes stocked as $CaCO_3$ microspheres (Istin and Masoni, 1973; Fournié and Chétail, 1982). The existence of electrochemical potential driving Ca^{2+} ions in the mantle from one epithelium to another is facilitated by the dead end geometry of the mantle at the shell edge (Fig. 7). The calcium carbonate precipitation produces one proton H^+ for each reacting Ca^{2+}. In order to avoid acidification, H^+ can be easily evacuated by proton channels, also largely widespread (Decoursey, 2003). Carbonate ions come either from metabolic CO_2 (which can readily cross membranes) or from external dissolved inorganic carbon (DIC) transferred by organic intermediates (Wheeler, 1992).

The role of calcium channels in metal incorporation has already been demonstrated for marine bivalves (Wang and Fisher, 1999) and for crustaceans (Rainbow, 1997). In particular, Sr^{2+} and Ba^{2+} can substitute for Ca^{2+} and diffuse through calcium channels (Hagiwara and Byerly, 1981; Friel and Tsien, 1989). Friel and Tsien (1989) experiments showed that Ba^{2+} discrimination is reduced when the ionic concentration gradient across the membrane increases. This effect can be expected to be stronger with Sr^{2+} ions since binding affinities in calcium channels are arranged as follows: $Ca^{2+} > Sr^{2+} > Ba^{2+}$ (Hagiwara and Byerly, 1981). Following theoretical models, if the electrochemical driving force for metallic ions entry is enhanced, the total ionic flux increases, reducing the tendency of Ca^{2+} to block other ions fluxes (Friel and Tsien, 1989; E.W. McCleskey, personal comm.). In our case, the driving force is the Ca^{2+} gradient induced by the mineralization activity. Therefore, the higher the mineralization rate, the easier Sr^{2+} ions cross the pores. At the level of a single channel, and with a first order approximation, the distribution coefficient D, as defined below, can be considered as linearly dependent on the total ionic flux j crossing the pore:

$$D = \beta j + a \qquad \text{with}$$

$$D = \frac{[Sr^{2+}]/[Ca^{2+}]_{\text{shellwards}}}{[Sr^{2+}]/[Ca^{2+}]_{\text{outwards}}},$$

and a, β constants, $\beta > 0$.

J is the Ca^{2+} flux per surface unit of calcifying epithelium. For a J value, the unitary flux j depends on n, the channel density per surface unit on the membranes. We consider the simple model where n is equal on each membrane of a same mantle section (Fig. 8)

$$J = nj.$$

Following Rosenberg et al. (1989) observations on metabolic gradients, the *M. donacium* calcifying mantle on short (curved) sections should have a density n_S lower than the density n_L on long sections ($n_L > n_S$). The calcium flux J is proportional to the crystal growth rate G:

$J = 0.4 \times G\rho/M_{Ca}$ with ρ, the aragonite density; and M_{Ca}, the calcium atomic mass.

Thus:

$$D = (\beta k/n)G + a \quad \text{with } k = 0.4 \times \rho/M_{Ca}.$$

This equation expresses the linear relationship between the Sr^{2+} distribution coefficient and the crystal growth rate. D_S is the distribution coefficient for short section calcium channels and D_L for long sections:

$$D_S = (\beta k/n_S)G_S + a; \quad D_L = (\beta k/n_L)G_L + a.$$

We measured the same crystal growth rate G on both sections, thus

$$D_S = (\beta k/n_S)G + a; \quad D_L = (\beta k/n_L)G + a.$$

These equations show that for a same G value, the discrimination against Sr^{2+} in a mantle area also depends on the calcium channel density n (Fig. 9), which may vary among species, individuals and inside shells. The lower the channel density in the epithelium, the more intense is the ionic flux in each channel, reducing the selectivity and increasing the dependence on growth rate. The model implies a biological variability: a large diversity exists among calcium channels which may have different chemical behaviours with metallic ions. The density and the distribution of cells having entry and exit channels also depend on species and individuals.

Our model provides a mechanism explaining the Sr/Ca dependence on growth rate observed by Stecher et al. (1996), Takesue and van Geen (2004) and Gillikin et al. (2005). The results obtained on *C. subrugosa* shells support

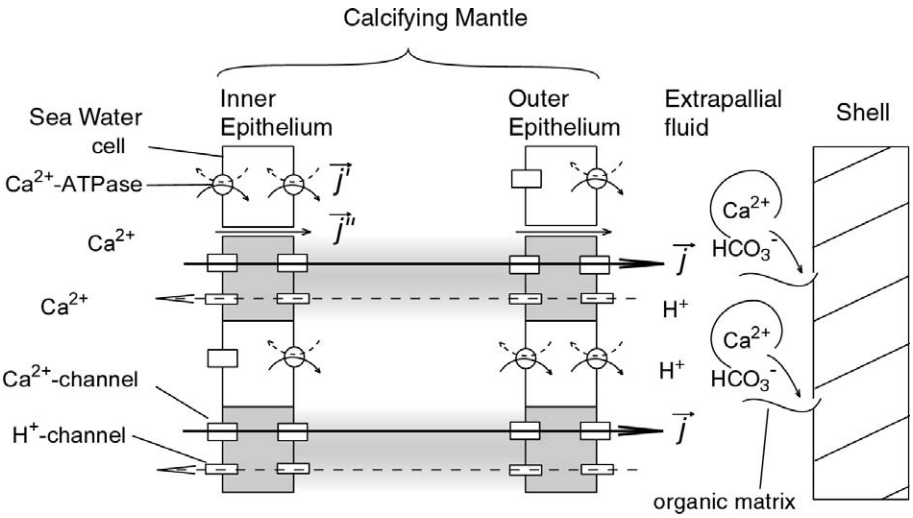

Fig. 8. Schematic calcification model for marine bivalve shells. Black arrows represent the Ca^{2+} fluxes and the dotted arrows represent the H^{+} fluxes. Three Ca^{2+} pathways through the mantle are shown: the major Ca^{2+}-channel pathway evidenced in gray (j), the metabolic pathway (j'), and the intercellular diffusive pathway (j''). Symbolic legend is indicated on the schema.

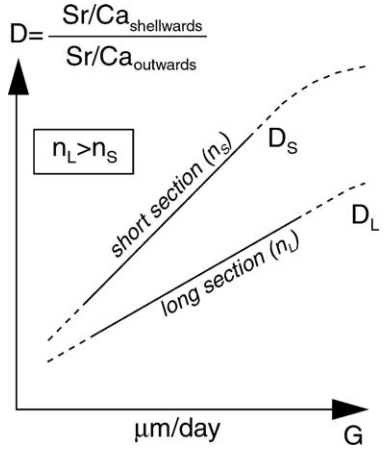

Fig. 9. Modelized relationship between the Sr distribution coefficient D across a single Ca^{2+}-channel and the crystal growth rate G on the facing mineralization front. The relationship is linear in the G range considered. D_S is the single-channel distribution coefficient in a short shell section, and D_L in a long shell section.

the proposed model. Both analysed shells exhibit a growth rate influence. The Sr/Ca values in shell PPCS1 are at the same time lower and less growth-dependent than in CM26-3 (Fig. 6), which can be explained by different Ca^{2+}-channel density on the epithelia. Our model is also coherent with the observations of Klein et al. (1996a): the slow growing shells have a lower Sr/Ca ratio than the rapidly growing shells. We suggest that the Sr/Ca measurements made in different *M. edulis* sections can also be explained by crystal growth rate differences. The mussel shape is extremely elongated compared to *M. donacium*, so that variation the section length is not only due to curvature but also to crystal growth. The slower crystal growth on the lateral mussel shell sections could account for their lower Sr/Ca values. Purton et al. (1999) observe in two mollusc shells (*Venericardia planicosta* and *Clavilithes macrospira*) an increasing trend in Sr/Ca ratios through ontogeny that seems at odds with our conclusions. However, for the bivalve *V. planicosta*, Sr/Ca ratios were measured in the nacreous layer (Fig. 7) where the calcification rate is much slower and the ion transport mechanism is different because of the inner position. Other influences are involved in this case, probably more metabolic as Purton et al. (1999) suggest. For the gastropod *C. macrospira*, we interpret the Sr/Ca increasing trend as a temperature effect (consistent with the $\delta^{18}O$ record) that is apparent because the mean annual growth rate remains very stable during the life period analysed (as can be inferred from the $\delta^{18}O$ record). Therefore, our calcification model can potentially reconcile the previous experimental results on marine molluscs. However, no generalization can be made, and further electrophysiological experiments of the mollusc mantle must be carried out to confirm our hypotheses.

5.4. Limits of model validity

5.4.1. Comparison with other calcifying organisms

The growth rate effect mechanism proposed here cannot be considered for every calcified tissue. As we suggested before, our model cannot account for Sr/Ca variations in mollusc nacreous layers, in shells with stable growth rate, or in very slow growing species which may not involve Ca^{2+}-channels in the ionic transport. Metal ions concentration in freshwater molluscs EPF is much higher than in the surrounding water, which implies a different ionic transport mechanism allowing ionic accumulation in the EPF. Calcification rate control on coralline aragonite Sr/Ca was also demonstrated (De Villiers et al., 1994). Although various studies suggested that Ca^{2+}-channels are involved in Ca^{2+} transport to the coralline skeleton (Ferrier-Pagès et al., 2002; Allemand et al., 2004), the growth rate effect in corals is different than in marine molluscs: (1) coral

Sr/Ca ratios are inversely correlated with calcification rate, and (2) Sr concentration is slightly higher in coralline aragonite than in sea water, whereas it is about twice lower in marine molluscs. The latter point suggests that the ionic transport in hermatypic corals is not selective. Therefore, calcification rate control on coral Sr/Ca probably happens during aragonite crystallization.

5.4.2. Other divalent cations

Ca^{2+}-channels selectivity against ions other than Ca^{2+} depends on the channel type, the binding site affinity for each ion species, and the fluid chemical composition both sides of the channel (Sather and McCleskey, 2003). Ca^{2+}-channel models often consider two binding sites in the pore. Ca^{2+} has the highest affinity and blocks the diffusion of other ions when occupying a binding site. The first Ca^{2+} ion is repulsively diffused by a second one (Hess and Tsien, 1984; Friel and Tsien, 1989; Gillespie and Eisenberg, 2002). Because of their high affinity, Sr^{2+} and Ba^{2+} are the best candidates to replace Ca^{2+} in Ca^{2+}-channels (Hagiwara and Byerly, 1981; Sather and McCleskey, 2003). Therefore, the mechanism proposed here for Sr^{2+} cannot be extended to every divalent metal ion. Ba^{2+} concentration in sea water is too low to compete with Ca^{2+} and Sr^{2+} and is probably incorporated by a metabolic pathway after ingestion, bound to suspended organic matter (Lazareth et al., 2003). The strong correlations observed in some cases between Sr/Ca and Ba/Ca do not necessary indicate similar pathways: a high growth rate is generally associated to high metabolic activity. Mn^{2+} and Mg^{2+} have low affinity with pore binding sites and are sometimes not permeant at all through Ca^{2+}-channels, so that these ions probably follow a different pathway.

6. Conclusions

We have shown for two marine bivalve species that the environmental parameters have minor influence on Sr, Ba, Mg and Mn concentration in shell aragonite. The well-defined sclerochronology of these species allows a precise study of the influence of crystal growth rate G on trace element incorporation, important in all shells, especially for Sr (explaining up to 74% of the Sr/Ca variance). The relationship between G and Sr/Ca exhibits variability among the shells as well as inside the shells. For a same growth rate value, Sr/Ca values are higher in more curved shell sections, and the growth rate influence is stronger as well.

We showed that intercellular and Ca^{2+}-pump pathways cannot support the calcification Ca^{2+} flux, leading us to propose an alternative mechanism for ionic transport through the calcifying mantle, implying a major role for calcium channels on epithelial cell membranes. Crystal growth rate has an effect on Sr^{2+} incorporation by determining the electrochemical potential driving the ions through the calcium channels. The stronger the potential, the lower the channel selectivity. This allows the Sr^{2+} ions to cross the membrane more easily. Variations of the calcium channel density on membranes can account for the G–Sr/Ca relationship variations. The model proposed here should be tested by physiological experiments on mollusc epithelium ionic permeability.

Acknowledgments

We are grateful to Dr. Marco Quiroz Ruiz, Ing. Freddy Cardenas, and all the colleagues from Instituto del Mar del Peru for their help. We deeply thank Dr. Luc Ortlieb for collecting modern *M. donacium* shells in Boca del Rio and Dr. Danièle Lavallée for the fossil shell. We also thank Oswaldo Perez and Jorge Maceda del Fondo Nacional de Desarollo Pesquero del Peru for their help in Puerto Pizarro. We thank Ricardo Rojas del Centro Nacional de Datos Oceanograficos de Chile for providing Africa temperature record.

Associate editor: Miryam Bar-Matthews

Appendix A. Supplementary data

Supplementary data associated with this article can be found, in the online version, at doi:10.1016/j.gca.2006.07.019.

References

Addadi, L., Moradian-Oldak, J., Furedimilhofer, H., Weiner, S., Veis, A., 1992. *Chemistry and Biology of Mineralized Tissues*. Elsevier, Amsterdam, pp. 153.

Allemand, D., Ferrier-Pages, C., Furla, P., Houlbrèque, F., Puverel, S., Reynaud, S., Tambutté, E., Tambutté, S., Zoccola, D., 2004. Biomineralisation in reef-building corals: from molecular mechanisms to environmental control. *Comptes Rendus Palevol* **3**, 453–467.

Beck, J.W., Edwards, R.L., Ito, E., Taylor, F.W., Recy, J., Rougerie, F., Joannot, P., Henin, C., 1992. Sea-surface temperature from coral skeletal Strontium/Calcium ratios. *Science* **257**, 644–647.

Belcher, A.M., Wu, X.H., Christensen, R.J., Hansmas, P.K., Stucky, G.D., Morse, D.E., 1996. Control of crystal phase switching and orientation by soluble mollusc-shell proteins. *Nature* **381**, 56–58.

Carpenter, S.J., Lohmann, K.C., 1992. Sr/Mg ratios of modern marine calcite: empirical indicators of ocean chemistry and precipitation rate. *Geochim. Cosmochim. Acta* **56**, 1837–1849.

Carré, M., 2005. Etude géochimique et sclérochronologique de coquilles de bivalves marins: paléocéanographie de la côte sud du Pérou à l'Holocène inférieur et implications archéologiques. unpublished PhD dissertation, Université Montpellier 2. pp. 348.

Carré, M., Bentaleb, I., Blamart, D., Ogle, N., Cardenas, F., Zevallos, S., Kalin, R.M., Ortlieb, L., Fontugne, M., 2005. Stable isotopes and sclerochronology of the bivalve *Mesodesma donacium*: potential application to peruvian paleoceanographic reconstructions. *Paleogeogr. Paleoclimatol. Paleoecol.* **228**, 4–25.

Chave, K.E., 1954. Aspects of biogeochemistry of magnesium. 1. Calcareous marine organisms. *J. Geol.* **62**, 266–283.

Cobb, K.M., Charles, C.D., Cheng, H., Edwards, R.L., 2003. El Niño/Southern oscillation and tropical Pacific climate during the last millennium. *Nature* **424**, 271–276.

Coimbra, J., Machado, J., Fernandes, P.L., 1988. Electrophysiology of the mantle of *Anodonta cygnea*. *J. Exp. Biol.* **140**, 65.

Corrège, T., Gagan, M.K., Beck, J.W., Burr, G.S., Cabioch, G., Le Cornec, F., 2004. Interdecadal variation in the extent of South Pacific tropical waters during the Younger Dryas event. *Nature* **428**, 927–929.

Dang, T.X., McCleskey, E.W., 1998. Ion channel selectivity through stepwise changes in binding affinity. *J. Gen. Physiol.* **111**, 185–193.

De Villiers, S., Shen, G.T., Nelson, B.K., 1994. The Sr/Ca–temperature relationship in coralline aragonite: influence of variability in $(Sr/Ca)_{seawater}$ and skeletal growth parameters. *Geochim. Cosmochim. Acta* **58**, 197–208.

Decoursey, T.E., 2003. Voltage-gated proton channels and other proton transfer pathways. *Physiol. Rev.* **83**, 475–579.

Dodd, J.R., 1965. Environmental control of strontium and magnesium in Mytilus. *Geochim. Cosmochim. Acta* **29** (5), 385–398.

Dodd, J.R., 1967. Magnesium and strontium in calcareous skeletons: a review. *J. Paleontol.* **41** (6), 1313–1329.

Dodd, J.R., Crisp, E.L., 1982. Non-linear variation with salinity of Sr/Ca and Mg/Ca ratios in water and aragonitic bivalve shells and implications for paleosalinity studies. *Paleogeogr. Paleoclimatol. Paleoecol.* **38**, 45–56.

Evans, J.W., 1975. Growth and micromorphology of two bivalves exhibiting non-daily growth lines. In: Rosenberg, G.D., Runcorn, S.K. (Eds.), *Growth Rythms and the History of the Earth's Rotation*. Wiley, New York, pp. 119–134.

Falini, G., Albeck, S., Weiner, S., Addadi, L., 1996. Control of aragonite or calcite polymorphism by mollusc shell macromolecules. *Science* **271**, 67–69.

Ferrier-Pagès, C., Boisson, F., Allemand, D., Tambutté, E., 2002. Kinetics of strontium uptake in the scleratinian coral *Stylophora pistillata*. *Mar. Ecol. Prog. Ser.* **245**, 93–100.

Fontugne, M., Usselmann, P., Lavallée, D., Julien, M., Hatté, C., 1999. El Nino variability in the coastal desert of southern Peru during the mid-holocene. *Quaternary Res.* **52**, 171–179.

Fournié, J., Chétail, M., 1982. Accumulation calcique au niveau cellulaire chez les mollusques. *Malacologia* **22** (1-2), 265–284.

Friel, D.D., Tsien, R.W., 1989. Voltage-gated calcium channels: direct observation of the anomalous mole fraction effect at the single-channel level. *Proc. Natl. Acad. Sci. USA* **86**, 5207–5211.

Gagan, M.K., Ayliffe, L.K., Beck, J.W., Cole, J.E., Druffel, E.R.M., Dunbar, R.B., Schrag, D.P., 2000. New views of tropical paleoclimates from corals. *Quaternary Sci. Rev.* **19**, 45–64.

Gillespie, D., Eisenberg, B., 2002. Physical descriptions of experimental selectivity measurements in ion channels. *Eur. Biophys. J.* **31**, 454–466.

Gillikin, D.P., Lorrain, A., Navez, J., Taylor, J.W., André, L., Keppens, E., Baeyens, W., Dehairs, F., 2005. Strong biological controls on Sr/Ca ratios in aragonitic marine bivalve shells. *Geochem. Geophys. Geosyst.* **6** (5), Q05009. doi:10.1029/2004GC000874.

Hagiwara, S., Byerly, L., 1981. Calcium channel. *Ann. Rev. Neurosci.* **4**, 69–125.

Hess, P., Tsien, R.W., 1984. Mechanism of ion permeation through calcium channels. *Nature* **309**, 453–456.

Istin, M., Kirschner, L.B., 1968. On the origin of the bioelectrical potential generated by the freshwater clam mantle. *J. Gen. Physiol.* **51**, 478–496.

Istin, M., Maetz, J., 1964. Perméabilité au calcium du manteau de lamellibranches d'eau douce étudiée à l'aide des isotopes ^{45}Ca et ^{47}Ca. *Biochim. Biohys. Acta* **88**, 227–230.

Istin, M., Masoni, A., 1973. Absorption et redistribution du calcium dans le manteau des lamellibranches en relation avec la structure. *Calcif. Tissue Res.* **11**, 151–162.

Kinsman, D.J., Holland, H.D., 1969. The coprecipitation of cations: IV. The coprecipitation of Sr^{2+} with aragonite between 16–96 °C. *Geochim. Cosmochim. Acta* **33**, 1–17.

Klein, R.T., Lohman, K.C., Thayer, C.W., 1996a. Sr/Ca and $^{13}C/^{12}C$ ratios in skeletal calcite of *Mytilus trossulus*: covariation with metabolic rate, salinity and carbon isotopic composition of sea water. *Geochim. Cosmochim. Acta* **60**, 4207–4221.

Klein, R.T., Lohman, K.C., Thayer, C.W., 1996b. Bivalve skeletons record sea-surface temperature and $\delta^{18}O$ via Mg/Ca and $^{18}O/^{16}O$ ratios. *Geology* **24** (5), 415–418.

Lavallée, D., Julien, M., Béarez, P., Usselman, P., Fontugne, M., Bolaños, A., 1999. Pescadores-recolectores arcaicos del extremo-sur Peruano. Excavaciones en la Quebrada de los Burros (Departamento de Tacna). Primeros resultados 1995–1997. *Bulletin de l'Institut Français d'Etude Andines* **28** (1), 1–11.

Lazareth, C.E., Vander-Putten, E., André, L., Dehairs, F., 2003. High-resolution trace element profiles in shells of the mangrove bivalve *Isognomon ephippium*: a record of environmental spatio-temporal variations? *Estuarine Coastal Shelf Sci.* **57**, 1103–1114.

Lorens, R.B., Bender, M.L., 1980. The impact of solution chemistry on *Mytilus edulis* calcite and aragonite. *Geochim. Cosmochim. Acta* **44**, 1265–1278.

Marin, F., Luquet, G., 2004. Molluscan shell proteins. *Comptes Rendus Palevol* **3**, 469–492.

Marshall, J.F., McCulloch, M.T., 2002. An assessment of the Sr/Ca ratio in shallow water hermatypic corals as a proxy for sea surface temperature. *Geochim. Cosmochim. Acta* **66** (18).

McWhirter, J.M., Gould, G.W., East, J.M., Lee, A.G., 1987. A kinetic model for Ca^{2+} efflux mediated by the $Ca^{2+} + Mg^{2+}$-activated ATPase of sarcoplasmic reticulum. *Biochem. J.* **245**, 713–722.

Milet, C., Berland, S., Lamghari, M., Mouries, L., Jolly, C., Borzeix, S., Doumenc, D., Lopez, E., 2004. Conservation of signal molecules involved in biomineralisation control in calcifying matrices of bone and shell. *Comptes Rendus Palevol* **3**, 493–501.

Neuilly, M., Cetama, 1998. *Modélisation et Estimation des erreurs de mesure*. Lavoisier Tec& Doc, Paris.

Pearce, N.J.G., Perkins, W.T., Westgate, J.A., Gorton, M.P., Jackson, S.E., Neal, C.R., Chenery, S.P., 1997. A compilation of new and published major and trace element data for NIST SRM 610 and NIST SRM 612 glass reference materials. *Geostandard Newslett.* **21**, 115–144.

Pilkey, O.H., Goodell, H.G., 1963. Trace element in recent mollusc shells. *Limnol. Oceanogr.* **8**, 137–148.

Purton, L.M.A., Shields, G.A., Brasier, M.D., Grime, G.W., 1999. Metabolism controls Sr/Ca ratios in fossil aragonitic mollusks. *Geology* **27** (12), 1083–1086.

Rainbow, P.S., 1997. Ecophysiology of trace metal uptake in crustaceans. *Estuarine Coastal Shelf Sci.* **44**, 169–175.

Rhoads, D.C., Lutz, R.A., 1980. *Skeletal Growth of Aquatic Organisms*. Plenum Press, New York.

Rosenberg, G.D., Hughes, W.W., 1991. A metabolic model for the determination of shell composition in the bivalve mollusc, *Mytilus edulis*. *Lethaia* **24**, 83–96.

Rosenberg, G.D., Hughes, W.W., Tkachuck, R.D., 1989. Shell form and metabolic gradients in the mantle of *Mytilus edulis*. *Lethaia* **22**, 343–344.

Rosenheim, B.E., Swart, P.K., Thorrold, S.R., 2005. Minor and trace elements in sclerosponge *Ceratoporella nicholsoni*: biogenic aragonite near the inorganic endmember? *Palaeogeogr. Palaeoclimatol. Palaeoecol.* **228**, 109–129.

Sather, W.A., McCleskey, E.W., 2003. Permeation and selectivity in calcium channels. *Ann. Rev. Physiol.* **65**, 133–159.

Stecher III, H.A., Krantz, D.E., Lord III, C.J., Luther III, G.W., Bock, K.W., 1996. Profiles of strontium and barium in *Mercenaria mercenaria* and *Spisula solidissima* shells. *Geochim. Cosmochim. Acta* **60** (18), 3445–3456.

Takesue, R.K., van Geen, A., 2004. Mg/Ca, Sr/Ca, and stable isotopes in modern and Holocene *Protothaca staminea* shells from a northern California coastal upwelling region. *Geochim. Cosmochim. Acta* **68** (19), 3845–3861.

Taylor, K.A., Dux, L., Martonosi, A., 1986. Three-dimensional reconstruction of negatively stained crystals of the Ca^{2+}-ATPase from muscle sarcoplasmic reticulum. *J. Mol. Biol.* **187** (3), 417–427.

Vander Putten, E., Dehairs, F., André, L., Baeyens, W., 1999. Quantitative in situ microanalysis of minor and trace elements in biogenic calcite using infrared laser ablation-inductively coupled plasma mass spectrometry: a critical evaluation. *Anal. Chim. Acta* **378**, 261–272.

Vander Putten, E., Dehairs, F., Keppens, E., Baeyens, W., 2000. High resolution distribution of trace elements in the calcite shell layer of modern *Mytilus edulis*: environmental and biological controls. *Geochim. Cosmochim. Acta* **64** (6), 997–1011.

Wada, K., Fujinuki, T., 1976. Biomineralization in bivalve molluscs with emphasis on the chemical composition of the extrapallial fluid. In: Watabe, N., Wilbur, K.M. (Eds.), *The Mechanisms of Mineralization in*

the Invertebrates and Plants. University of South Carolina Press, pp. 175–190.

Wang, W.-X., Fisher, N.S., 1999. Effects of calcium and metabolic inhibitors on trace element uptake in two marine bivalves. *J. Exp. Marine Biol. Ecol.* **236**, 149–164.

Wheeler, A.P., 1992. Mechanisms of molluscan shell formation. In: Bonucci, E. (Ed.), *Calcification in Biological Systems*. CRC press, Boca Raton, pp. 179–216.

Wheler, A.P., George, J.W., Evans, C.A., 1981. Control of calcium carbonate nucleation and crystal growth by soluble matrix of oyster shell. *Science* **212**, 1397–1398.

Wilbur, K.M., Saleuddin, A.S.M., 1983. Shell formation. In: Saleuddin, A.S.M., Wilbur, K.M. (Eds.), *The Mollusca*, vol. 4. Academic Press, New York, pp. 235–287.

Yu, K.F., Zhao, J.X., Wei, G.J., Cheng, X.R., Chen, T.G., Felis, T., Wang, P.X., Liu, T.S., 2005. $\delta^{18}O$, Sr/Ca and Mg/Ca records of Porites lutea corals from Leizhou peninsula, northern South China Sea, and their applicability as paleoclimatic indicators. *Paleogeogr. Paleoclimatol. Paleoecol.* **218**, 57–73.

Zhong, S., Mucci, A., 1989. Calcite and aragonite precipitation from sea water solutions of various salinities: precipitation rates and overgrowth compositions. *Chem. Geol.* **78**, 283–299.